PROTEINS: Structure, Function, and Genetics 42:77–84 (2001)

Helix Nucleation Kinetics From Molecular Simulations in Explicit Solvent

Gerhard Hummer,[1*] Angel E. García,[2] and Shekhar Garde[3]
[1]*Laboratory of Chemical Physics, National Institute of Diabetes and Digestive and Kidney Diseases, National Institutes of Health, Bethesda, Maryland*
[2]*Theoretical Biology and Biophysics Group T-10, Los Alamos National Laboratory, Los Alamos, New Mexico*
[3]*Department of Chemical Engineering, Rensselaer Polytechnic Institute, Troy, New York*

ABSTRACT **We study the reversible folding/unfolding of short Ala and Gly-based peptides by molecular dynamics simulations of all-atom models in explicit water solvent. A kinetic analysis shows that the formation of a first α-helical turn occurs within 0.1–1 ns, in agreement with the analyses of laser temperature jump experiments. The unfolding times exhibit Arrhenius temperature dependence. For a rapidly nucleating all-Ala peptide, the helix nucleation time depends only weakly on temperature. For a peptide with enthalpically competing turn-like structures, helix nucleation exhibits an Arrhenius temperature dependence, corresponding to the unfolding of enthalpic traps in the coil ensemble. An analysis of structures in a "transition-state ensemble" shows that helix-to-coil transitions occur predominantly through breaking of hydrogen bonds at the helix ends, particularly at the C-terminus. The temperature dependence of the transition-state ensemble and the corresponding folding/unfolding pathways illustrate that folding mechanisms can change with temperature, possibly complicating the interpretation of high-temperature unfolding simulations. The timescale of helix formation is an essential factor in molecular models of protein folding. The rapid helix nucleation observed here suggests that transient helices form early in the folding event. Proteins 2001;42:77–84.**

INTRODUCTION

The kinetics of protein folding is increasingly seen as a key to elucidating the mechanisms that guide the self-assembly of proteins into their folded structure.[1–26] This growing interest in protein folding kinetics continues to stimulate the development of fast, time-resolved spectroscopic methods to probe the earliest, submicrosecond events in protein folding.[14,21,27,28] At the same time, molecular simulations of proteins in water—although still too expensive computationally for routine studies of millisecond (or even microsecond) folding events—are increasingly overlapping with the timescales of those fastest experiments, as shown by folding simulations extending beyond a microsecond[29,30] and extensive studies of the equilibrium folding kinetics of a β-peptide,[31,32] or by the mapping of protein free energy surfaces.[26,33]

These exciting developments both on the experimental and on the computational side have reinvigorated an analysis of fundamental steps in protein folding, in particular the formation of secondary structure, such as α-helices and β-turns.[17,34–45] One of the key results of the experimental studies is that α-helix formation, a fundamental element of protein folding, was shown to occur over a nanosecond timescale.[46,47] However, this fast rate of helix formation was recently questioned on the basis of stopped-flow circular dichroism (CD) experiments that indicate a timescale of 0.1 s for helix formation,[48] about six orders of magnitude slower than the earlier laser temperature jump experiments.[46,47] These recent results question not only the laser T jump studies but also mechanisms of protein folding that require early formation of native-like secondary structure, because mostly helical proteins, such as a λ repressor fragment, were shown to fold in as fast as 20 μs,[16] four orders of magnitude faster than the timescale of helix formation found by CD.[48]

In helix-coil theory,[49–52] forming the first helical turn stabilized by (i, i, + 4) backbone hydrogen bonds nucleates a helix, followed by helix propagation. Here, we use molecular simulations to study this initial phase of helix formation. From the equilibrium dynamics of blocked penta-peptides in explicit water, we determine the timescales of forming and breaking the first helical turn. The simulations cover a broad range in temperature and time and explore variations in the peptide sequence.

MATERIALS AND METHODS

We perform molecular dynamics (MD) simulations to study reversible helix nucleation of the simplest peptide sequences that can form 1.5 turns of α-helix with three (i, i + 4) backbone hydrogen bonds: Ac-Ala_5-NHMe (A_5), Ac-Ala_2-Gly-Ala_2-NHMe (A_2GA_2), and Ac-Gly_5-NHMe (G_5). These peptides are simulated in explicit solvent at temperatures from 250 K to 400 K for about 10 ns per run. The MD simulations of the peptides A_5, A_2GA_2, and G_5 are performed by using the AMBER 4.1 program[53] and the all-atom AMBER 94 force field.[54] The 1–4 interactions are

*Correspondence to: Gerhard Hummer, Laboratory of Chemical Physics, Bldg. 5, National Institute of Diabetes and Digestive and Kidney Diseases, National Institutes of Health, Bethesda, MD 20892-0520. E-mail: hummer@helix.nih.gov

Received 1 May 2000; Accepted 29 August 2000

TABLE I. Length of MD Production Runs in Nanoseconds

T [K]	A_5	A_2GA_2	G_5
250	11.6	—	—
275	12.8	—	—
300	12.0	13.4	10.0
350	13.4	12.5	—
400	7.8	4.8	—

consistently scaled by a factor of 1/1.2. The peptides are immersed into an aqueous solvent containing 500 (A_2GA_2), 499 (A_5), and 461 (G_5) TIP3P water molecules,[55] respectively. All simulations are performed under periodic boundary conditions. Long-range electrostatic interactions are treated by using the particle-mesh-Ewald (PME) method.[56] A grid of $32 \times 32 \times 32$ points is used in the PME calculations, resulting in a grid width of about 0.8 Å. A third-order spline interpolation is used with a real-space tolerance factor DSUM_TOL = 1.1×10^{-6}. A time step of 2 fs is used in the MD simulations, constraining the length of bonds involving hydrogen atoms by using the SHAKE algorithm.[57] The size of the cubic box is equilibrated at constant pressure (1 bar) and temperature by using the Berendsen coupling algorithm.[58] The production runs are performed at constant volume and temperature, with configurations saved for analysis every 1 ps. The length of the production runs is compiled in Table I.

The peptide sequences used in the simulations are $CO(CH_3)$-Ala_5-$NH(CH_3)$, $CO(CH_3)$-Ala_2-Gly-Ala_2-$NH(CH_3)$, and $CO(CH_3)$-Gly_5-$NH(CH_3)$, with acetyl and N-methyl blocking groups neutralizing the ends. This results in 30, 29, and 25 heavy atoms (C, N, O) and 32, 30, and 22 hydrogen atoms for A_5, A_2GA_2, and G_5, respectively. Fully extended peptides are energy minimized in vacuo and then solvated. Water molecules that overlapped with atoms of the peptide are removed. The solvated systems are equilibrated for at least 100 ps at 300 K. The simulations at temperatures different from 300 K are started from structures taken from the 300-K run, which are then equilibrated at constant pressure for at least 100 ps.

RESULTS

Principal-Component Analysis of Peptide Conformation Space

To quantify the kinetics of helix nucleation, we first identify a helical reference structure based on a principal-component axes (PCA) projection[59,60] of the peptide conformation spaces (Fig. 1) applied recursively. This recursive use of PCA analysis is suggested by the observation of a hierarchical structure in the energy landscape of proteins.[61] The structures within $2\,k_BT$ of the minimum in the free energy surface of the first *three* PCA components of A_5 at 300 K are subjected to a second round of PCA analysis. Four additional rounds of PCA analysis are conducted by using the structures within $1\,k_BT$ of the previously found minimum (i.e., we include regions x_{PCA} of PCA conformation space with a PCA conformation-space density of $\rho(x_{PCA})/\max[\rho(x_{PCA})] > e^{-1}$ in successive rounds of PCA analysis). The structures remaining after this recursive PCA analysis are highly homogeneous, and their average is a helical structure shown in Figure 2. The backbone dihedral angles (φ,ψ) for Ala_1 to Ala_5 of this reference structure are (−57.4, −45.3), (−64.0, −40.9), (−63.9, −41.9), (−63.4, −37.8), and (−70.9, −23.8) in units of degrees.

The multidimensional free energy surfaces projected onto the first two PCAs show strikingly different characteristics for the three peptides (Fig. 1). G_5 shows an essentially featureless free energy surface in the PCA plane. This is indicative of the absence of a dominant structure class for the G_5 peptide. In particular, no appreciable fraction of helical structures is found for G_5. The free energy surface of A_5, on the other hand, is dominated by a deep minimum that corresponds to α-helical structures. The minimum is at the bottom of a funnel-like free energy surface. The A_2GA_2 peptide has the most structured free energy surface with a primary helical minimum. Additional minima are located within the coil region of the free energy surface. In particular, a substantial population of turn-like structures[62,63] (Fig. 3) results from the flexibility of the central Gly residue.

Helix Nucleation Kinetics

Figure 4 shows the root-mean-square distance (RMSD) from the helical reference structure for A_5 as a function of time for temperatures between 250 K and 400 K. RMSDs were calculated for the heavy atoms of the backbone, excluding hydrogen and C_β atoms. The features of the RMSD time series suggest a multitude of two-state like (helix-coil) transformations from low RMSD to high RMSD and vice versa. Relaxation occurs on the subnanosecond timescale, except at 300 K where a fully extended peptide conformation (RMSD > 3 Å) occurred only once and did not relax for about 1 ns. Fully extended structures of A_5 did not occur at lower temperatures (250 K, 275 K) and relaxed rapidly at higher temperatures (350 K, 400 K). Figure 5 shows the distributions of RMSDs from the helical reference structure at 300 K for peptides A_5, A_2GA_2, and G_5. The distributions are sharply peaked at small RMSDs for the A_5 and A_2GA_2 peptides. We thus define the helical ensemble as the conformations within 0.6 Å RMSD from the helical reference structure, corresponding to the first peak in the RMSD distributions of A_5 and A_2GA_2 (Fig. 2). The kinetics of helix nucleation is then determined from the interconversion between helical (RMSD < 0.6 Å) and coil states (RMSD ≥ 0.6 Å).

Figure 6 shows the mean first passage times (MFPT) for helix nucleation and helix-to-coil transitions. MFPTs are defined as the average time to reach the dividing surface (RMSD = 0.6 Å) between coil and helix states from an equilibrium distribution in the coil and helix ensembles, respectively. The most striking result is that helix nucleation occurs rapidly on a timescale of 0.1 ns for A_5, and 0.1–1 ns for A_2GA_2. This is consistent with helix formation times of near 100 ns for peptides of about 20 amino acids, as determined from laser T jump measurements with infrared and fluorescence probes,[46,47] and in contrast to CD data suggesting a helix formation time of about 0.1 s

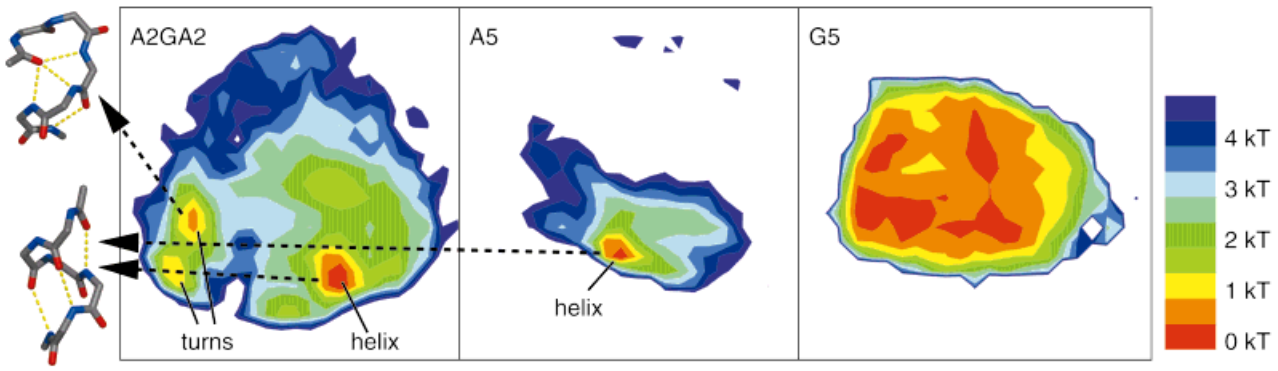

Fig. 1. Free energy profiles in the plane of the first (horizontal axis) and second PCA (vertical axis) of the peptides A_2GA_2 (**left**), A_5 (**middle**), and G_5 (**right**) at 300 K. The color coding indicates free energy differences to the respective minimum in units of k_BT. Shown on the left are the backbones of the helical reference structure (**bottom**) and of a turn structure (**top**), corresponding to minima in the free energy surfaces.

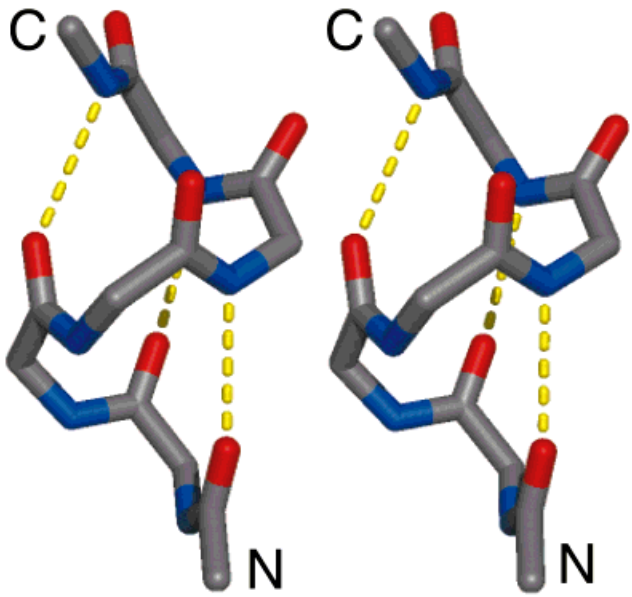

Fig. 2. Stereo view of the helical reference structure of peptide A5. Shown are the heavy backbone atoms with carbon atoms in gray, oxygen atoms in red, and nitrogen atoms in blue. Dotted yellow lines indicate backbone hydrogen bonds. N and C indicate the N and C-terminus of the peptide.

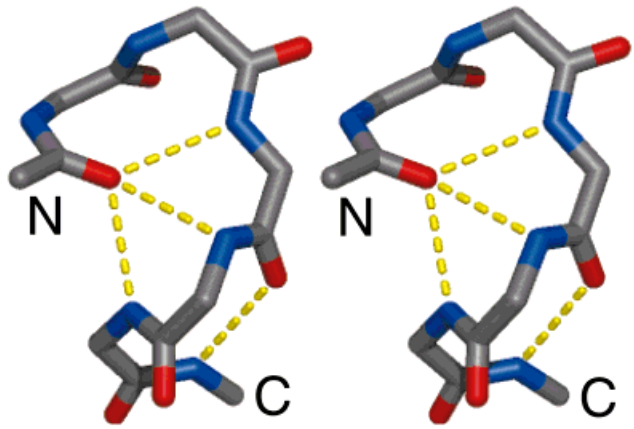

Fig. 3. Stereo view of one of the turn structures corresponding to the figure-eight shaped minimum in the PCA plane of A_2GA_2 (Fig. 1). See Figure 2 for details.

for a 16 amino acid peptide.[48] Quantitative support for subnanosecond helix nucleation times comes from a detailed kinetic analysis of helix-coil transition experiments: Thompson et al.[64] estimate the relaxation time for nucleating a first helical turn in a 21-residue Ala peptide to be < 0.1 ns, starting from an all-coil state. Tobias and Brooks[65] estimated helix initiation times for Ac-Ala_3-NMe of about 100 ps from a kinetic interpretation of calculated free energy differences between extended, turn, and helical structures. Subnanosecond timescales have also been observed for turn formation of penta and hexapeptides.[41,43] A kinetic interpretation of the Zimm-Bragg model for the helix coil transition, with barriers derived from free energy simulations, led to estimated helix formation times in the 10–100 ns range,[66] as measured in T jump experiments with infrared and fluorescence probes.[46,47]

Helix nucleation is significantly faster for A_5 than for A_2GA_2. Furthermore, the MFPTs for helix nucleation of A_5 are practically temperature independent over the range studied here (250 K $< T <$ 400 K), whereas those of A_2GA_2 exhibit Arrhenius behavior. Temperature-independent helix formation rates were indeed deduced from a two-state analysis of the experimental[64] helix relaxation kinetics (J. Hofrichter, personal communication). Figure 6 shows that helix-to-coil transitions are only slightly faster for A_2GA_2 than for A_5. Both A_5 and A_2GA_2 exhibit Arrhenius-like behavior for helix-to-coil transitions, MFPT $\sim \exp(\Delta H^{\ddagger}/k_BT)$, with similar enthalpic barriers of $\Delta H^{\ddagger} = 13.9 \pm 1$ and 10.9 ± 2 kJ mol^{-1}, respectively (neglecting the temperature dependence of the solvent viscosity). These results strongly suggest a thermally activated process for the helix-to-coil transitions of both A_5 and A_2GA_2. Helix nucleation of A_5, on the other hand, is dominated by a diffusive search in the coil state, with transitions into the helical state over a small free energy barrier (k_BT or less).[67]

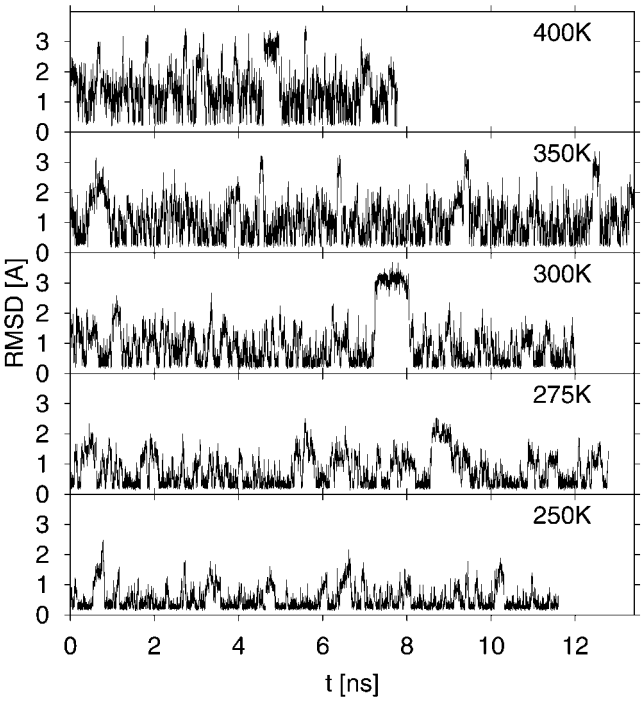

Fig. 4. RMSD of A_5 from the helical reference structure as a function of time for temperatures between 250 and 400 K.

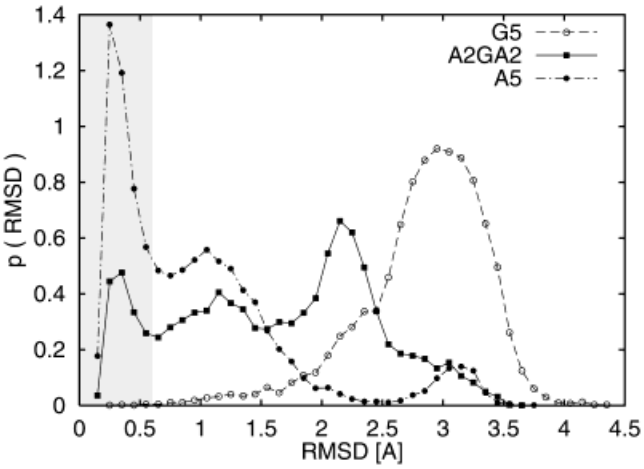

Fig. 5. Probability distribution of the RMSD from the helical reference structure at 300 K. The shaded region of RMSD below 0.6 Å defines the helical state.

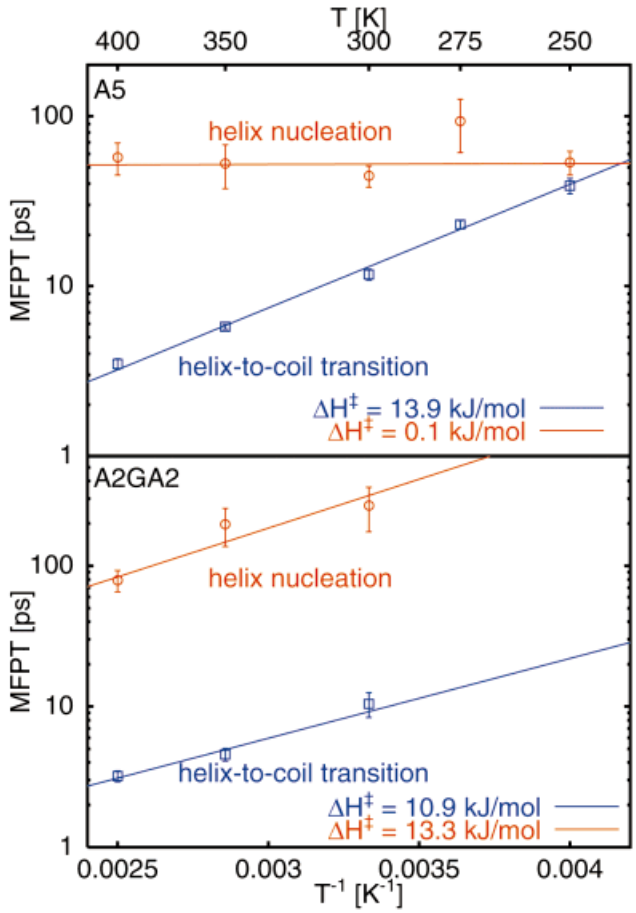

Fig. 6. Temperature dependence of MFPTs for helix nucleation (red) and helix-to-coil transitions (blue) of A_5 (top) and A_2GA_2 (bottom). Helix nucleation and helix-to-coil transition times are shown as circles and squares, respectively. The lines are fits to Arrhenius models, MFPT $\sim \exp(\Delta H^{\ddagger}/k_B T)$.

For A_2GA_2, unlike A_5, the MFPTs for helix nucleation depend on temperature. The PCA analysis of the A_2GA_2 conformation space (Fig. 1) suggests that this temperature dependence of the helix nucleation MFPTs arises from "unfolding" of enthalpically stabilized "trap" conformations rather than crossing of an activation barrier close to the helical state. We investigate this by studying the "unfolding" rates from the figure-eight shaped minimum in the A_2GA_2 PCA plane shown in Figure 1. A conformation of A_2GA_2 is considered to belong to that state when it has < 0.5 Å RMSD from one of the two turn-like reference structures defined by PCA analysis of the figure-eight shaped minimum. With this definition, we find that the MFPT for escape from this "folding trap" has an Arrhenius temperature dependence with an activation enthalpy of about 10.4 $\pm$ 1 kJ mol^{-1}. This activation enthalpy for escape from a "trap" conformation agrees well with the apparent activation enthalpy of 13.3 $\pm$ 4 kJ mol^{-1} for helix nucleation of A_2GA_2, as shown in Figure 6. With identical helix-to-coil transition times of A_5 and A_2GA_2 (Fig. 6), we conclude that the effect of changing the central Ala residue to Gly affects only the coil side of the equilibrium through introduction of "folding traps," but not the helical side. The role of enthalpic traps in determining the folding times of heteropeptides is discussed below.

Transition-State Ensemble

We now attempt to characterize the "pathways" of helix formation and unfolding. We define a "*transition-state ensemble*" as those coil conformations (i.e., with RMSD from the helical reference structure > 0.6 Å) that were helical either at the 1-ps snapshot before or after, by using the A_5 trajectory at 350 K. With that definition, we capture

TABLE II. Backbone Hydrogen-Bond Distances (in Å Units) Between Carbonyl Oxygen and Amide Nitrogen Atoms of the Structures Participating in the Transition-State Ensemble (Columns 2–5)†

	O_1N_5	O_2N_6	O_3N_7	O_3N_6	250 K	275 K	300 K	350 K	400 K
1	3.1	3.5	5.2	4.0	0.65	0.57	0.50	0.40	0.31
2	4.6	3.2	3.3	3.5	0.20	0.23	0.25	0.25	0.24
3	3.0	5.0	3.2	3.2	0.08	0.09	0.11	0.12	0.10
4	3.1	3.1	3.2	4.0	0.02	0.03	0.04	0.09	0.15
h	3.0	3.1	3.2	3.5	0.01	0.02	0.02	0.02	0.02
o					0.03	0.05	0.08	0.13	0.19

†Also listed is the fraction at which these structures participate in the transition-state ensemble for temperatures between 250 and 400 K (columns 6–10). The first column lists the four structure classes identified through recursive PCA analysis. Also included are the helical (h) and other (o) structure classes. Residues 1 and 7 are the acetyl and N-methyl blocking groups, respectively. Underlined numbers are highlighting broken hydrogen bonds with O-N distances exceeding 3.5 Å, respectively.

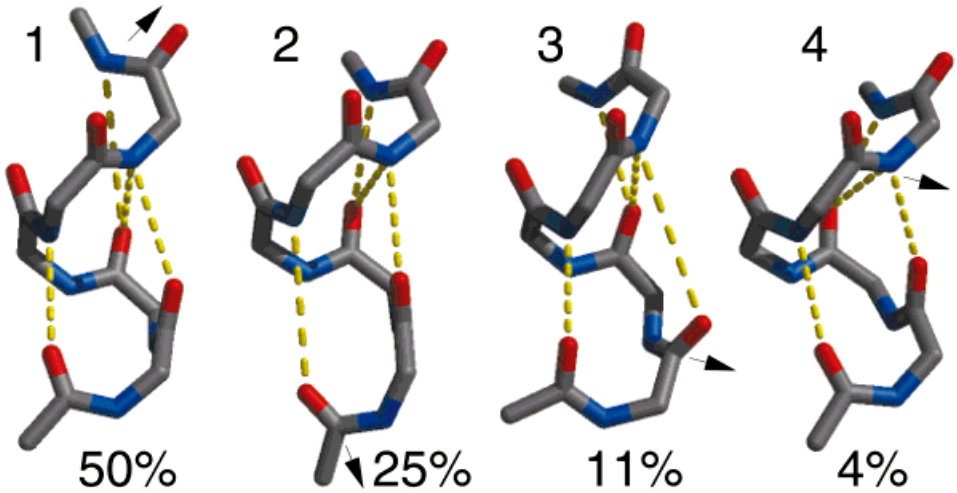

Fig. 7. Reference structures of the transition-state ensemble for helix formation and unfolding. The four structures are numbered as in Table II. Arrows indicate the dominant motion relative to the helical reference structure shown in Figure 2. The percentage numbers at the bottom indicate the relative participation in the A_5 transition-state ensemble at 300 K. See Figure 2 for details.

those coil peptide conformations that convert most rapidly into or from a helical state. The structures within 1 ps of the helical state are analyzed by using PCA.[59,60] In a PCA representation using the first three PCA components, we identify four distinct conformations as part of this transition-state ensemble. A recursive PCA analysis defines reference structures for each of the four conformational basins. These structures have distinct backbone hydrogen-bonding features, as summarized in Table II and shown in Figure 7.

For every conformation of the transition-state ensemble we have calculated the RMSD from the four reference structures and the helical structure. A reference structure is then assigned on the basis of the smallest RMSD. If the minimum RMSD exceeded 0.7 Å, we did not assign a structure. With that definition, we can partition the transition-state ensemble at 300 K to about 92%. The dominant structure in the transition-state ensemble has the C-terminal (i, i + 4) hydrogen bond broken (50%). The second-most prevalent structure (25%) has the N-terminal (i, i + 4) hydrogen bond broken. About 12% of the structures in the transition-state ensemble have the central (i, i + 4) hydrogen bond broken. Approximately 9% of the structures lost the weak, bifurcated C-terminal (i, i + 3) hydrogen bond. A recent NMR study[68] indicated a significant population of (i, i + 3) hydrogen bonds at helix termini of alanine-based peptides and corresponding 3_{10} helices, which have been implicated as intermediates in the helix-coil transition.[69] (i, i + 3) hydrogen bonds as intermediates in helix formation and breakage were also incorporated into kinetic models of helix formation.[65,70]

The composition of the transition-state ensemble suggests that helix formation and unfolding occur predominantly through addition or breaking of a single hydrogen bond. The C-terminal hydrogen bond appears to be the most fragile, resulting either in breaking (structure 1 in Table II and Fig. 7) or loss of its weakly bifurcated character (structure 4 in Table II and Fig. 7). The central hydrogen bond is the most protected. Preferential unfolding of α-helices from the C-terminal end was observed in earlier MD simulations.[38,39,40] Based on free energy calculations, this effect could be attributed to solvent interac-

tions favoring C-terminal unfolding.[71] The temperature-dependent composition of the transition-state ensemble listed in Table II indicates that breaking of the C-terminal (i, $i + 4$) hydrogen bond dominates particularly at low temperatures, whereas at higher temperature loss of its bifurcated character gains in importance, as does breaking of the N-terminal (i, $i + 4$) hydrogen bond. This suggests an entropic contribution to the relative weighting of folding/unfolding pathways.

CONCLUSIONS

From molecular simulations of blocked penta-peptides in water, we conclude that the initial step in helix nucleation is fast, on the order of 0.1–1 ns, depending on sequence and temperature. Although this is anticipated from fast, time-resolved experiments using infrared and fluorescence probes of helix-coil transitions,[46,47,64] it appears to contradict recent CD studies[48] that found helix formation rates of about 15 s^{-1}. Our results suggest a significant influence of the amino acid sequence on the helix nucleation kinetics through the introduction of enthalpically stabilized conformations into the coil state. In addition, transient hydrophobic interactions between the aliphatic parts of lysine side chains in the coil state of the AK peptide[48] could result in slower helix formation. Increased hydrophobic effects with increasing temperature[72,73] (0–60°C) would partly explain the observed reduction in relaxation rates with increasing temperature.[48] However, a difference of six orders of magnitude in experimental helix formation times[46–48] (10^{-7} vs. 10^{-1} s) cannot easily be accounted for by variations in peptide length and sequence. Thus, further experiments are required to resolve this discrepancy.

An analysis of the sequence dependence of helix nucleation reveals surprising similarities to protein folding models. Within the energy-landscape description of protein folding, the all-Ala peptide can be classified as a "fast-folding" peptide, where the helix nucleation kinetics is determined by downhill diffusion in conformation space without a significant free energy barrier to the helical state.[3,74] Substituting the central Ala by Gly introduces enthalpically stabilized "traps" into the coil state. Helix nucleation in A_2GA_2 thus requires a combination of activated escape from these enthalpically trapped conformations and subsequent conformational diffusion. Similar effects may be expected for heteropolymers where hydrophobic contacts not leading to the helical state can increase the helix formation time. This highlights the role of non-native interactions in the unfolded state of proteins.[75,76]

Although a Gly substitution at the center of the peptide slows down the helix nucleation kinetics, the helix-to-coil transition is unaffected. We find that helix breaking requires a thermally activated escape from an enthalpically stabilized helical state. The height of the enthalpic barrier is similar in the A_5 and A_2GA_2 peptides, suggesting that it derives from breaking the backbone hydrogen bonds and not hydrophobic interactions or dihedral angle barriers. This is further supported by an analysis of the transition-state ensemble. In agreement with earlier studies,[38–40,71] we find that unfolding occurs predominantly through breaking of single hydrogen bonds at the helix ends, with the C-terminal hydrogen bond being the most fragile.

The weighting of specific unfolding pathways exhibits a considerable temperature dependence, reflecting entropic components in the corresponding transition-state free energies. This finding highlights possible difficulties in extrapolating results of high-temperature unfolding simulations to room temperature. Because the transition state ensemble itself depends on temperature, temperature changes affect not only the timescales but also relative weights of different folding/unfolding pathways.

We emphasize that equilibrium simulations, such as those reported here, bring experimental and theoretical studies of biomolecular dynamics and folding to closer overlap. Although direct comparisons between time-resolved experiments and simulations are affected by the definition of states (helical and coil), future simulation studies might aim directly at reproducing measured quantities, such as time-dependent infrared absorbance, fluorescence, or ellipticity. This will offer unique opportunities: on one hand, we can use the experimental constraints to fine-tune potential parameterizations; on the other hand, the atomic resolution of molecular simulations will help interpret and guide experiments.

ACKNOWLEDGMENTS

We thank William A. Eaton, Attila Szabo, R. Brian Dyer, J. Hofrichter, and José N. Onuchic for many stimulating discussions. Computer access to the Los Alamos ASCI Nirvana supercomputer through an IHPCI grant is gratefully acknowledged.

REFERENCES

1. Bryngelson JD, Wolynes PG. Intermediates and barrier crossing in a random energy model (with applications to protein folding). J Phys Chem 1989;93:6902–6915.
2. Leopold PE, Montal M, Onuchic JN. Protein folding funnels a kinetic approach to the sequence structure relationship. Proc Natl Acad Sci USA 1992;89:8721–8725.
3. Onuchic JN, Luthey-Schulten Z, Wolynes PG. Theory of protein folding the energy landscape perspective. Annu Rev Phys Chem 1997;48:545–600.
4. Onuchic JN, Nymeyer H, García AE, Chahine J, Socci ND. The energy landscape theory of protein folding: insights into folding mechanisms and scenarios. Adv Prot Chem 2000;53:87–152.
5. Kim PS, Baldwin RL. Intermediates in the folding reactions of small proteins. Annu Rev Biochem 1990;59:631–660.
6. Šali A, Shakhnovich E, Karplus M. How does a protein fold? Nature 1994;369:248–251.
7. Dill KA, Bromberg S, Yue KZ, et al. Principles of protein folding: a perspective from simple exact models. Protein Sci 1995;4:561–602.
8. Dill KA, Chan HS. From Levinthal to pathways to funnels. Nat Struct Biol 1997;4:10–19.
9. Guo ZY, Thirumalai D. Kinetics of protein folding: nucleation mechanism, time scales, and pathways. Biopolymers 1995;36:83–102.
10. Camacho CJ, Thirumalai D. Kinetics and thermodynamics of folding in model proteins. Proc Natl Acad Sci USA 1993;90:6369–6372.
11. Scheraga HA, Hao MH. Entropy sampling Monte Carlo for polypeptides and proteins. Adv Chem Phys 1999;105:243–272.
12. Jones CM, Henry ER, Hu Y, et al. Fast events in protein folding

initiated by nanosecond laser photolysis. Proc Natl Acad Sci USA 1993;90:11860–11864.
13. Sabelko J, Ervin J, Gruebele M. Observation of strange kinetics in protein folding. Proc Natl Acad Sci USA 1999;96:6031–6036.
14. Dyer RB, Gai F, Woodruff WH. Infrared studies of fast events in protein folding. Acc Chem Res 1998;31:709–716.
15. Fersht AR, Matouschek A, Serrano L. The folding of an enzyme. 1. Theory of protein engineering analysis of stability and pathway of protein folding. J Mol Biol 1992;224:771–782.
16. Burton RE, Huang GS, Daugherty MA, Calderone TL, Oas TG. The energy landscape of a fast-folding protein mapped by Ala→Gly substitutions. Nat Struct Biol 1997;4:305–310.
17. Dyson HJ, Wright PE. Insights into protein folding from NMR. Annu Rev Phys Chem 1996;47:369–395.
18. Bai YW, Sosnick TR, Mayne L, Englander SW. Protein folding intermediates native-state hydrogen-exchange. Science 1995;269: 192–197.
19. Roder H, Colón W. Kinetic role of early intermediates in protein folding. Curr Opin Struct Biol 1997;7:15–28.
20. Baker D. Metastable states and folding free energy barriers. Nat Struct Biol 1998;5:1021–1024.
21. Eaton WA, Muñoz V, Thompson PA, Henry ER, Hofrichter J. Kinetics and dynamics of loops, α-helices, β-hairpins, and fast-folding proteins. Acc Chem Res 1998;31:745–753.
22. Pascher T, Chesick JP, Winkler JR, Gray HB. Protein folding triggered by electron transfer. Science 1996;271:1558–1560.
23. Jennings PA, Wright PE. Formation of a molten globule intermediate early in the kinetic folding pathway of apomyoglobin. Science 1993;262:892–896.
24. Lazaridis T, Karplus M. New view of protein folding reconciled with the old through multiple unfolding simulations. Science 1997;278:1928–1931.
25. Nymeyer H, García AE, Onuchic JN. Folding funnels and frustration in off-lattice minimalist protein landscapes. Proc Natl Acad Sci USA 1998;95:5921–5928.
26. Boczko EM, Brooks CL. First-principles calculation of the folding free energy of a 3 helix bundle protein. Science 1995;269:393–396.
27. Gruebele M, Sabelko J, Ballew R, Ervin J. Laser temperature-jump induced protein refolding. Acc Chem Res 1998;31:699–707.
28. Lednev IK, Karnoup AS, Sparrow MC, Asher SA. α-helix peptide folding and unfolding activation barriers a nanosecond UV resonance Raman study. J Am Chem Soc 1999;121:8074–8086.
29. Duan Y, Kollman PA. Pathways to a protein folding intermediate observed in a 1 microsecond simulation in aqueous solution. Science 1998;282:740–744.
30. Duan Y, Wang L, Kollman PA. The early stage of folding of villin headpiece subdomain observed in a 200-nanosecond fully solvated molecular dynamics simulation. Proc Natl Acad Sci USA 1998;95: 9897–9902.
31. Daura X, Jaun B, Seebach D, van Gunsteren WF, Mark AE. Reversible peptide folding in solution by molecular dynamics simulation. J Mol Biol 1998;280:925–932.
32. Daura X, van Gunsteren WF, Mark AE. Folding-unfolding thermodynamics of a β-heptapeptide from equilibrium simulations. Prot Struct Funct Genet 1999;34:269–280.
33. Bursulaya BD, Brooks CL. Folding free energy surface of a three-stranded beta-sheet protein. J Am Chem Soc 1999;121:9947–9951.
34. Blanco FJ, Rivas G, Serrano L. A short linear peptide that folds into a native stable β hairpin in aqueous solution. Nat Struct Biol 1994;1:584–590.
35. Muñoz V, Thompson PA, Hofrichter J, Eaton WA. Folding dynamics and mechanism of β-hairpin formation. Nature 1997;390:196–199.
36. Chakrabartty A, Baldwin RL. Stability of α-helices. Adv Prot Chem 1995;46:141–176.
37. Rossky PJ, Karplus M. Solvation: a molecular dynamics study of a dipeptide in water. J Am Chem Soc 1979;101:1913–1937.
38. Soman KV, Karimi A, Case DA. Unfolding of an α-helix in water. Biopolymers 1991;31:1351–1361.
39. Tirado-Rives J, Jorgensen WL. Molecular dynamics simulations of the unfolding of an α helical analog of ribonuclease A S-peptide in water. Biochemistry 1991;30:3864–3871.
40. Daggett V, Levitt M. Molecular-dynamics simulations of helix denaturation. J Mol Biol 1992;223:1121–1138.
41. Tobias DJ, Mertz JE, Brooks III CL. Nanosecond time scale folding dynamics of a pentapeptide in water. Biochemistry 1991;30: 6054–6058.
42. Brooks III CL, Case DA. Simulations of peptide conformational dynamics and thermodynamics. Chem Rev 1993;93:2487–2502.
43. Mohanty D, Elber R, Thirumalai D, Beglov D, Roux B. Kinetics of peptide folding computer simulations of SYPFDV and peptide variants in water. J Mol Biol 1997;272:423–442.
44. Pande VS, Rokhsar DS. Molecular dynamics simulations of unfolding and refolding of a β-hairpin fragment of protein G. Proc Natl Acad Sci USA 1999;96:9062–9067.
45. Klimov DK, Thirumalai D. Mechanisms and kinetics of β-hairpin formation. Proc Natl Acad Sci USA 2000;97:2544–2549.
46. Williams S, Causgrove TP, Gilmanshin R, et al. Fast events in protein folding: helix melting and formation in a small peptide. Biochemistry 1996;35:691–697.
47. Thompson PA, Eaton WA, Hofrichter J. Laser temperature-jump study of the helix-coil kinetics of an alanine peptide interpreted with a kinetic zipper model. Biochemistry 1997;36:9200–9210.
48. Clarke DT, Doig AJ, Stapley BJ, Jones GR. The α-helix folds on the millisecond time scale. Proc Natl Acad Sci USA 1999;96:7232–7237.
49. Zimm BH, Bragg JK. Theory of the phase transition between helix and random coil in polypeptide chains. J Chem Phys 1959;31:526–535.
50. Lifson S, Roig A. On the theory of helix-coil transition in polypeptides. J Chem Phys 1961;34:1963–1974.
51. Poland D, Scheraga HA. Theory of helix-coil transitions in biopolymers. New York: Academic Press; 1970.
52. Qian H, Schellman JA. Helix-coil theories: a comparative-study for finite length polypeptides. J Phys Chem 1992;96:3987–3994.
53. Pearlman DA, Case DA, Caldwell JW, et al. AMBER 4.1. San Francisco: University of California; 1995.
54. Cornell WD, Cieplak P, Bayley CI, et al. A second generation force field for the simulation of proteins, nucleic acids, and organic molecules. J Am Chem Soc 1995;117:5179–5197.
55. Jorgensen WL, Chandrasekhar J, Madura JD, Impey RW, Klein ML. Comparison of simple potential functions for simulating liquid water. J Chem Phys 1983;79:926–935.
56. Darden T, York D, Pedersen L. Particle mesh Ewald: an $N \cdot \log(N)$ method for Ewald sums in large systems. J Chem Phys 1993;98: 10089–10092.
57. Ryckaert JP, Cicotti G, Berendsen HJC. Numerical integration of Cartesian equations of motion of a system with constraints: molecular dynamics of n-alkanes. J Comput Phys 1977;23:327–341.
58. Berendsen HJC, Postma JPM, van Gunsteren WF, Nola AD, Haak JR. Molecular dynamics with coupling to an external bath. J Chem Phys 1984;81:3684–3690.
59. García AE. Large-amplitude nonlinear motions in proteins. Phys Rev Lett 1992;68:2696–2699.
60. García AE, Blumenfeld R, Hummer G, Krumhansl JA. Multi-basin dynamics of a protein in a crystal environment. Physica D 1997;107:225–239.
61. Ansari A, Berendzen J, Bowne SF, Frauenfelder H, Iben IET, Shyamsunder E, Young RD. Protein states and proteinquakes. Proc Natl Acad Sci USA 1985;82:5000–5004.
62. Wilmot CM, Thornton JM. Analysis and prediction of the different types of β-turn in proteins. J Mol Biol 1988;203:221–232.
63. Yang AS, Hitz B, Honig B. Free energy determinants of secondary structure formation. 3. Beta-turns and their role in protein folding. J Mol Biol 1996;259:873–882.
64. Thompson PA, Muñoz V, Jas GS, Henry ER, Eaton WA, Hofrichter J. The helix-coil kinetics of a heteropeptide. J Phys Chem B 2000;104:378–389.
65. Tobias DJ, Brooks CL III. Thermodynamics and mechanism of α helix initiation in alanine and valine peptides. Biochemistry 1991;30:6059–6070.
66. Brooks III CL. Helix-coil kinetics: folding time scales for helical peptides from a sequential kinetic model. J Phys Chem 1996;100: 2546–2549.
67. Hummer G, García AE, Garde S. Conformational diffusion and helix formation kinetics. Phys Rev Lett 2000;85:2637–2640.
68. Millhauser GL, Stenland CJ, Hanson P, Bolin KA, Vandeven FJM. Estimating the relative populations of 3_{10}-helix and α helix in Ala-rich peptides a hydrogen exchange and high field NMR study. J Mol Biol 1997;267:963–974.
69. Sundaralingam M, Sekharudu YC. Water-inserted α-helical seg-

ments implicate reverse turns as folding intermediates. Science 1989;244:1333–1337.
70. Sheinerman FB, Brooks CL III. 3_{10}-Helices in peptides and proteins as studied by modified Zimm-Bragg theory. J Am Chem Soc 1995;117:10098–10103.
71. Young WS, Brooks III CL. A microscopic view of helix propagation: N and C-terminal helix growth in alanine helices. J Mol Biol 1996;259:560–572.
72. Garde S, Hummer G, García AE, Paulaitis ME, Pratt LR. Origin of entropy convergence in hydrophobic hydration and protein folding. Phys Rev Lett 1996;77:4966–4968.
73. Garde S, García AE, Pratt LR, Hummer G. Temperature dependence of the solubility of non-polar gases in water. Biophys Chem 1999;78:21–32.
74. Hardin C, Luthey-Schulten Z, Wolynes PG. Backbone dynamics, fast folding, and secondary structure formation in helical proteins and peptides. Prot Struct Funct Genet 1999;34:281–294.
75. Creamer TP, Srinivasan R, Rose GD. Modeling unfolded states of peptides and proteins. Biochemistry 1995;34:16245–16250.
76. Dill KA, Shortle D. Denatured states of proteins. Annu Rev Biochem 1991;60:795–825.